Comptes Rendus

Physique

Sébastien Lalléchère, Lala Rajaoarisoa, Laurent Clavier, Raul Sanchez Galan and Blaise Ravelo

Bandpass NGD function design for 5G microwave signal delay synchronization application

URSI-France 2020 Workshop / *Journées URSI-France 2020*

Bandpass NGD function design for 5G microwave signal delay synchronization application

Sébastien Lalléchère ® *, ᵃ, **Lala Rajaoarisoa** ® ᵇ, **Laurent Clavier** ® ᵇ,
Raul Sanchez Galan ᶜ **and Blaise Ravelo** ® ᶜ

ᵃ Université Clermont Auvergne, Institut Pascal, SIGMA Clermont, France

ᵇ IMT Lille Douai, Institut Mines-Télécom, Univ. Lille, Centre for Digital Systems,
F-59000 Lille, France

ᶜ Nanjing University of Information Science & Technology (NUIST), Nanjing,
Jiangsu 210044, China

E-mails: sebastien.lallechere@uca.fr (S. Lalléchère), lala.rajaoarisoa@imt-lille-douai.fr
(L. Rajaoarisoa), laurent.clavier@imt-lille-douai.fr (L. Clavier), r.galan@reading.ac.uk
(R. S. Galan), blaise.ravelo@nuist.edu.cn (B. Ravelo)

Abstract. This paper introduces a design method of simple bandpass (BP) negative group delay (NGD) topology. The fundamental specifications of BP NGD function are defined. The NGD passive topology consists of parallel resistance associated with an open-ended microstrip stub. The NGD properties and characterization with respect to the constituting stub parameters are established. The validations are performed with theoretical calculated and simulated GD, transmission and reflection coefficients. The BP NGD circuit can be useful for the improvement of phase linearity and GD equalization of future 5G microwave devices.

Keywords. Negative group delay (NGD), Bandpass (BP) NGD function, Design method, Microstrip 5G circuit, NGD analysis and synthesis.

Available online 6th May 2021

1. Introduction

The twenty-first century differs from the previous ones under the incessant increase of tremendous communications initially between mankind. Following the different socio-economic needs, the communications were extended between mankind-object and even object-object [1]. The modern communication system is expected to operate under the master word target wireless connection "anything, anywhere and anytime". The scenario of a future 5G smart city proposed by 5G IA shown in Figure 1 illustrates the necessity of connected infrastructure, things and people [1].

---

* Corresponding author.

Figure 1. Architecture and scenario of 5G infrastructure proposed by 5G IA [1] (Permission granted by 5G IA).

To set this 5G city, significant technological race on 5G architecture requiring a higher data rate and higher bandwidth is currently open between developed countries (US, China, EU, …) [2]. 5G technological advancement is expected as a promising solution for future mobile communication [3]. However, the communication system using 5G wireless sensor networks (WSNs) may suffer from electromagnetic compatibility (EMC) issues, for example, due to the radio link signal interferences [4, 5], EMC and massive Internet of Things (IoT) [6].

Different challenging RF and microwave device designs have been made to be under the race for the future 5G infrastructure deployment. For example, to improve the performances of the transmitter (Tx) and receiver (Rx) circuits, a reconfigurable phased array was introduced for controlling 5G terminals [7]. High directive beam steering of adaptive antenna array plays an important role in the performance of such communication terminals [8].

An innovative solution of phased array design, using the unfamiliar negative group delay (NGD) function, enabling beam squint elimination was proposed [9–12]. Such a phased array design method is fundamentally based on the use of NGD based non-Foster elements [13–15]. The NGD non-Foster networks were initially designed with lossy circuits which limit their fields of potential applications [13, 14]. Then, active circuit based non-Foster elements were also designed [15]. In addition to the phased array networks, the NGD circuits were also used for the design of oscillators, filters [16] and phase shifter [17] for RF and microwave communication systems. Moreover, the NGD function was also used for the design of diverse devices as an absorptive band-stop filter [18] and equalization of bandpass filters [19]. One of the most specific applications of NGD function concerns the signal delay compensation [20] and propagation delay synchronisation [21]. This later application is implemented with the reduction of the propagation delay based on the NGD function [21]. Despite these tentative applications, so far, the familiarity of non-specialist RF and microwave engineers to the NGD function necessitates further research works. For this reason, the present paper is focused on the design method of bandpass NGD circuit for 5G frequency band. Before the elaboration of the circuit design, it is worth noticing a brief description of microwave NGD state of the art.

The NGD microwave existence was one of the curious debates between research design engineers in the 2000s. Different feasibility of NGD effect generations [22–33] was investigated. The NGD effect was experimented with signal interference techniques [22]. Then, the NGD function was also designed with a microwave transversal filter approach [23]. The democratization of the NGD function was also be proven with its different aspects as the possibility of dual-band design [24]. The most promising NGD applications were encouraged by the number of research works on the compact and miniaturized microstrip transmission line (TL) circuit designs per-
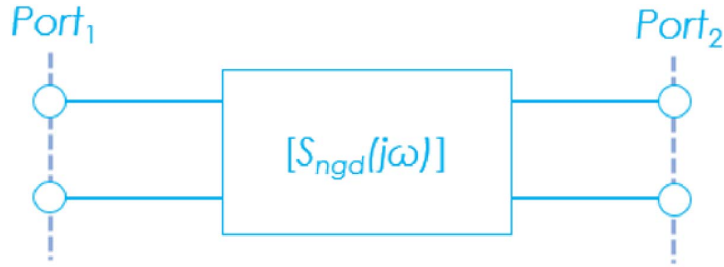
Figure 2. Two-port black box microwave system.

formed in the last decade [25–30].

Because of the unfamiliarity of RF/microwave design engineers and also research communities to this fascinating function, it would be necessary to highlight the NGD function meaning. In this way, the analogy between the filter and NGD functions was initiated in [31, 32]. The concept of bandpass (BP) NGD function was introduced as a function of the sign of the transmission coefficient group delay (GD) [32]. Because of the open-stub based NGD topology simplicity, a design of a BP NGD cell with 5G-centre frequency was recently proposed during URSI France scientific days 2020 [33]. This paper is an extension of the research work published in [33] with further detailed description of the BP NGD specifications, theoretical design and potential applications.

2. Preliminary definition of bandpass NGD function

A preliminary definition of the unfamiliar BP NGD function is introduced in this section. After the theoretical expression recall, the specification parameters will be defined. The key parameters required for the NGD study will be pedagogically explored.

2.1. *S-matrix black box*

First and foremost, acting as a two-port system, the NGD circuit investigated in the present paper can be generalized by the black box system represented in Figure 2. By denoting the complex angular frequency variable, $s = j\omega$, this system can be analytically modelled by the 2-D S-matrix:

$$[S_{\mathrm{NGD}}(j\omega)] = \begin{bmatrix} S_{11}(j\omega) & S_{12}(j\omega) \\ S_{21}(j\omega) & S_{22}(j\omega) \end{bmatrix}. \tag{1}$$

In contrast to the classical RF and microwave circuits, the NGD study requires more intensive analysis of frequency responses of GD calculated from the S-matrix introduced in (1).

2.2. *Magnitudes of S-parameters*

Before the NGD analytical definition, it is worth noting that the present paper is essentially focused on passive circuits. Therefore, the performance assessment of BP NGD circuit must include:

- The insertion loss or gain related to the transmission coefficient magnitude which should be lower than an expected value, $a < 1$:

$$S_{21}(\omega) = |S_{21}(j\omega)| \geq a \tag{2}$$

- The input and output reflection losses related to the reflection coefficient magnitudes which must be lower than an expected matching value, $b < 1$:

$$S_{11}(\omega) = |S_{11}(j\omega)| \leq b \tag{3}$$

$$S_{22}(\omega) = |S_{22}(j\omega)| \leq b. \tag{4}$$

2.3. *Transmission GD definition*

By its definition, the NGD study is fundamentally dependent on the GD analytical expression. For this reason, it would be important to recall the mathematical definition of this key parameter. It is derived from the phase of the transmission coefficient of S-matrix introduced in (1). In other words, it is given by:

$$\varphi(\omega) = \arg[S_{21}(j\omega)]. \tag{5}$$

The analytical model of the associated GD is defined by:

$$GD(\omega) = \frac{-\partial \varphi(\omega)}{\partial \omega}. \tag{6}$$

2.4. *Graphical representation of BP NGD specifications*

The unfamiliar BP NGD function was inspired by BP filter response [31, 32]. However, it is important to note that the NGD function depends essentially on the sign of GD expressed in (6) but not the behaviour of the S_{21} magnitude. By taking:

$$\omega_{m=1,2} = 2\pi f_m \tag{7}$$

the type of NGD function depends on the frequency band position, $\omega_1 \leq \omega \leq \omega_2$, where we have:

$$GD(\omega_1 \leq \omega \leq \omega_2) \leq 0. \tag{8}$$

Figure 3(a) illustrates an ideal GD response of BP NGD function. The main specifications can be defined:

- By taking a real positive delay, t, the GD value:

$$GD(\omega_1 \leq \omega \leq \omega_2) = -t \tag{9}$$

- NGD bandwidth:

$$\Delta\omega = 2\pi\Delta f = \omega_2 - \omega_1 \tag{10}$$

- NGD centre frequency:

$$\Delta\omega_0 = 2\pi f_0 \in [\omega_1, \omega_2] \tag{11}$$

- As illustrated in Figure 3(b), through dB-value $-a_{dB} = 20\log 10(a)$, the reflection coefficient:

$$S_{11}(\omega_1 \leq \omega \leq \omega_2) = a. \tag{12}$$

- And as explained in Figure 3(c), through dB-value $-b_{dB} = 20\log 10(b)$, the transmission coefficient:

$$S_{21}(\omega_1 \leq \omega \leq \omega_2) = b. \tag{13}$$

3. Bandpass NGD theoretical investigation on open-ended passive topology

The present section describes the theoretical approach of the BP NGD circuit. The present study details essentially the analytical investigation reported in [33].
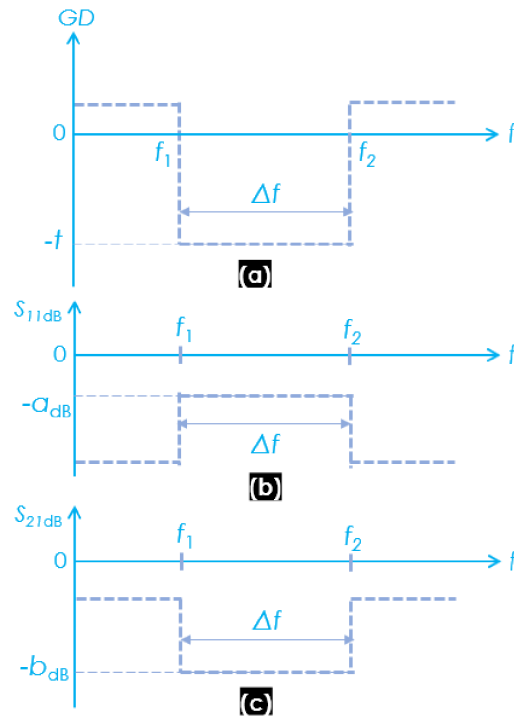
Figure 3. BP NGD function ideal specification: (a) GD, (b) S_{11} and (c) S_{21}.

3.1. *Topological description*

Figure 4 represents the TL based topology of NGD passive cell connected between node M and ground node [16]. This topology is assumed connected to terminal reference impedances, $R_0 = 50\,\Omega$ connected between nodes M_1M and MM_2. The circuit can be represented as a two-port system fed by voltage sources U_1 (left) and U_2 (right). It induces the input currents, I^1 and I^2. Meanwhile, the equivalent impedance, $[Z_{\text{NGD}}(j\omega)]$, is linked to the external voltage and current vectors by the matrix relation:

$$\begin{bmatrix} U_1(j\omega) \\ U_2(j\omega) \end{bmatrix} = [Z_{\text{NGD}}(j\omega)] \begin{bmatrix} I^1(j\omega) \\ I^2(j\omega) \end{bmatrix}. \tag{14}$$

The topology under study is essentially composed of a parallel resistance R ended by a lossless open-ended stub $\text{TL}(Z, \tau_0)$ which is defined by characteristic impedance Z and delay τ_0.

Acting as a lossless TL, the input impedance can be defined as [17]:

$$Z_{\text{in}}(j\omega) = R + \frac{Z}{j\tan(\omega\tau_0)} \tag{15}$$

Meanwhile, the equivalent impedance, $[Z_{\text{NGD}}(j\omega)]$, can be written as:

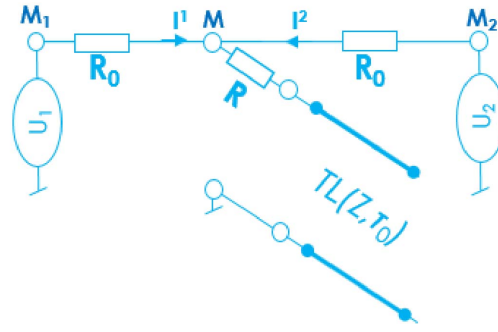$$[Z_{\text{NGD}}(j\omega)] = \frac{\begin{bmatrix} 1 & 1 \\ 1 & 1 \end{bmatrix}}{Z_{\text{in}}(j\omega)}. \tag{16}$$

Figure 4. Open-ended stub based NGD passive circuit.

3.2. *S-matrix frequency response*

The equivalent S-matrix can be extracted from Z-to-S transform:

$$[S_{\text{NGD}}(j\omega)] = ([Z_{\text{NGD}}(j\omega)] - R_0[1_2]) \times ([Z_{\text{NGD}}(j\omega)] + R_0[1_2])^{-1} \tag{17}$$

where:

$$[1_2] = \begin{bmatrix} 1 & 0 \\ 0 & 1 \end{bmatrix}. \tag{18}$$

The analytical development of this matrix relationship enables us to determine the S-matrix of our circuit. Subsequently, we emphasize that the S-matrix must be symmetric and its elements must satisfy the relations:

$$S_{12}(j\omega) = S_{21}(j\omega) = \frac{2Z_{\text{in}}(j\omega)}{R_0 + 2Z_{\text{in}}(j\omega)} \tag{19}$$

$$S_{11}(j\omega) = S_{22}(j\omega) = \frac{-R_0}{R_0 + 2Z_{\text{in}}(j\omega)}. \tag{20}$$

It can be demonstrated that the reflection and transmission coefficient responses of the proposed topology can be written as:

$$S_{11}(j\omega) = \frac{R_0 \tan(\omega\tau_0)}{2jZ - (2R + R_0)\tan(\omega\tau_0)} \tag{21}$$

$$S_{21}(j\omega) = \frac{2[jZ - R\tan(\omega\tau_0)]}{2jZ + (2R + R_0)\tan(\omega\tau_0)}. \tag{22}$$

The associated magnitudes are expressed as, respectively:

$$S_{11}(\omega) = |S_{11}(j\omega)| = \frac{R_0|\tan(\omega\tau_0)|}{\sqrt{(2R + R_0)^2 \tan^2(\omega\tau_0) + 4Z^2}} \tag{23}$$

$$S_{21}(\omega) = |S_{21}(j\omega)| = \frac{2\sqrt{Z^2 + R^2 \tan^2(\omega\tau_0)}}{\sqrt{(2R + R_0)^2 \tan^2(\omega\tau_0) + 4Z^2}}. \tag{24}$$

3.3. *NGD analysis*

Before the NGD analysis, it is worth recalling the GD analytical expression. The mathematical condition between the NGD topology parameters is expressed. The analysis demonstrating why the proposed topology can be classified as a BP NGD function is presented.

3.3.1. *GD of the considered passive topology*

First, as a reminder to (5), the transmission phase associated to expression (21) is written as:

$$\varphi(\omega) = -\arctan\left[\frac{Z}{R\tan(\omega\tau_0)}\right] - \arctan\left[\frac{2Z}{(2R+R_0)\tan(\omega\tau_0)}\right]. \tag{25}$$

The GD of the open-ended stub cell introduced in Figure 4 can be derived from (6) and the previous transmission phase. As a matter of fact, we have the detailed analytical expression of the open-ended stub topology GD:

$$\mathrm{GD}(\omega) = \frac{R_0 Z \tau_0 [1 + \tan^2(\omega\tau_0)][2Z^2 - R(2R+R_0)\tan^2(\omega\tau_0)]}{[Z^2 + R^2\tan^2(\omega\tau_0)][2Z^2 + (2R+R_0)^2\tan^2(\omega\tau_0)]}. \tag{26}$$

3.3.2. *NGD existence condition*

The GD expressed in (25) satisfies the condition:

$$\mathrm{GD}(\omega) \leq 0 \tag{27}$$

Equivalently, this inequality can be expressed as:

$$2Z^2 - R(2R+R_0)\tan^2(\omega\tau_0) \leq 0. \tag{28}$$

In other words, this inequality can be transformed as:

$$\tan^2(\omega\tau_0) \geq \frac{2Z^2}{R(2R+R_0)} \Rightarrow \tan(\omega\tau_0) \geq \frac{Z\sqrt{2}}{\sqrt{R(2R+R_0)}}. \tag{29}$$

From the latter inequality, the NGD bandwidth is derived:

$$\Delta f = \left\{\frac{\omega_0}{\pi} - \frac{2}{\tau_0}\arctan\left[\frac{Z\sqrt{2}}{\sqrt{R(R_0+2R)}}\right]\right\}. \tag{30}$$

3.3.3. *Analysis at the particular frequency, $\omega = \omega_0$*

The NGD analysis consists in proving that the proposed passive topology is capable of operating as a BP NGD function. Doing this, we intuitively have the NGD centre frequency:

$$f_0 = \frac{\omega_0}{2\pi}. \tag{31}$$

Acting as quarter wave length TL, this characteristic frequency can be expressed as a function of the propagation delay:

$$f_0 = \frac{0.25}{\tau_0}. \tag{32}$$

At this particular frequency, it can be established that the S-parameters established in (22) and (23) become, respectively:

$$S_{11}(\omega_0) = |S_{11}(j\omega_0)| = \frac{R_0}{2R+R_0} \tag{33}$$

$$S_{21}(\omega_0) = |S_{21}(j\omega_0)| = \frac{2R}{2R+R_0}. \tag{34}$$

It means that the reflection coefficient is intrinsically linked to the transmission coefficient by the relationship:

$$S_{11}(\omega_0) = 1 - S_{21}(\omega_0). \tag{35}$$

Furthermore, the GD expressed in (26) is simplified as:

$$\mathrm{GD}(\omega_0) = \frac{-R_0 Z \tau_0}{R(R_0+2R)}. \tag{36}$$

3.4. *NGD design synthesis equations of the proposed open-ended stub topology in function of given specifications*

Similar to the classical filter or amplifier or other microwave circuits, the specifications of the BP NGD function introduced earlier in Figure 3 are necessary to design the unknown circuit (see Figure 4).

3.4.1. *Equation of TL delay*

The desired NGD centre frequency, f_0, is the main parameter to determine the propagation delay of TL constituting our BP NGD circuit introduced in Figure 4. The analytical equation can be transited from (32). Therefore, we have the synthesis equation:

$$\tau_0 = \frac{0.25}{f_0}. \tag{37}$$

3.4.2. *Equation of R*

To determine the resistor, R, of the open-ended stub topology introduced in Figure 4, we need the value of return loss, $a < 1$. Generally, to fulfil the matching expectation, $a = -10$ dB is considered for standard microwave circuits. Therefore, the unknown resistor can be obtained by solving the equation:

$$S_{11}(f_0) = a. \tag{38}$$

In this case, as predicted by (35), the transmission coefficient is systematically:

$$S_{21}(f_0) = 1 - a. \tag{39}$$

Emphatically, we can establish the synthesis equation:

$$R = \frac{0.5R_0(1-a)}{a}. \tag{40}$$

3.4.3. *Equation of TL characteristic impedance*

The design equation of the TL characteristic impedance, Z, can be established from the given propagation delay, which needs to be reduced from BP NGD circuit. We can denote for example this delay by the real positive, $t > 0$. The resolution of the following equation enables to determine the synthesis formula of this impedance:

$$\text{GD}(f_0) = -t. \tag{41}$$

Accordingly, we can demonstrate from expression (36) that the characteristic impedance synthesis equation of NGD circuit introduced in Figure 4 is:

$$Z = \frac{0.5R_0(1-a)t}{a^2\tau_0}. \tag{42}$$

4. BP NGD validation results and delay reduction application principle

This section is focused on the validation of the previous BP NGD theory. Doing this, a proof of concept (POC) designed with microstrip circuit is introduced. The ideal circuit synthesis from previously established design formulas will be introduced. Then, the comparison between the ideal model and commercial tool simulation is discussed.
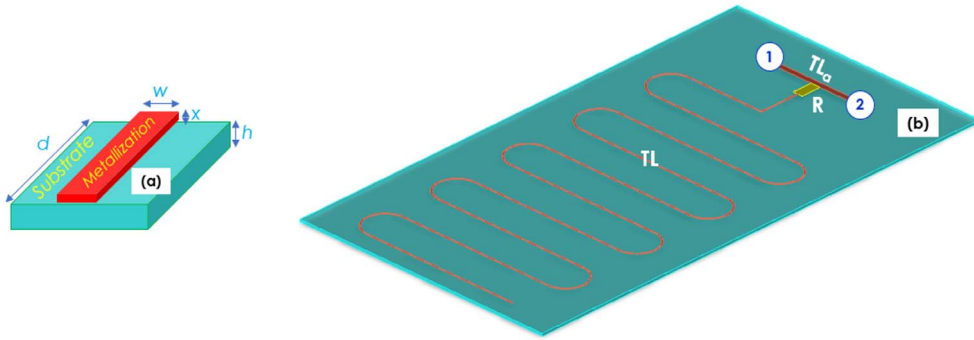
Figure 5. (a) Microstrip design and (b) NGD circuit POC 3D design.

Table 1. Specifications of the NGD microstrip circuit

Structure	Designation	Parameter	Value
Dielectric substrate	Kapton	—	—
	Relative permittivity	ε_r	3.3
	Loss tangent	$\tan(\delta)$	0.002
	Height	h	125 μm
Conductor metallization	Copper	—	—
	Conductivity	σ	58 MS/s
	Thickness	t	17 μm

4.1. *POC description*

As POC, microstrip circuits were designed and simulated to validate more concretely the previously developed BP NGD theory. The geometrical parameters of the microstrip structure is illustrated in Figure 5(a). The dielectric substrate is supposed characterized by thickness, h and the Copper-metallized conductor supposed is characterized by physical width w, length d and thickness x. Figure 5(b) shows the 3D design of the NGD circuit POC constituted by:

- Resistor, R,
- Terminated by an open-ended, $\text{TL}(w, d)$ having physical width, w, and physical length, d, and,
- Access lines $\text{TL}_a(w_a, d_a)$ having physical width, w_a, and physical length, d_a.

The specifications of the Kapton substrate and metallization of the NGD circuit POC are indicated in Table 1.

4.2. *Discussion on the obtained results*

This subsection explores the validation results of the open-ended stub-based BP NGD theory. It is noteworthy that the analytical Matlab calculations of the BP NGD circuit ideal model were realized with:

- Reflection coefficient given in (22),
- Transmission coefficient carried out from (23),
- And GD from (25).

To validate the analytical calculated results, the POC circuit introduced in Figure 5(b) was simulated with the commercial tool ADS® from Keysight Technologies® schematic environment.

Table 2. BP NGD specifications to operate at 3.6 GHz

Designation	Name	Value
NGD centre frequency	f_0	3.6 GHz
Delay	t	0.34 ns
Reflection loss	$-a_{dB}$	10 dB

Table 3. Calculated parameters for the ideal BP NGD circuit

Designation	Name	Value
Resistor	R	60 Ω
TL delay	τ_0	69 ps
TL characteristic impedance	Z	1 kΩ

Table 4. Specifications of the NGD microstrip circuit

Element	Designation	Name	Value
Stub TL	Width	w	62 μm
	Length	d	23.4 cm
Resistor	Resistor	R	60 Ω
Access line	Width	w_a	277 μm
	Length	d_a	2 mm

4.2.1. *3.6-GHz BP NGD POC*

Table 2 addresses the desired NGD specifications to design the 5G NGD POC with 3.6 GHz centre frequency. By using design (37), (40) and (42), we obtain the NGD parameters summarized in Table 3.

The present computational study was carried out in the bandwidth from f_{min} = 3.3 GHz to f_{max} = 3.9 GHz under more than 200 samples.

Parametric analyses were performed in function of resistor, R, and the TL characteristic impedance, Z. Figures 6(a), 6(b) and 6(c) display the cartographies of GD, S_{11} and S_{21}, respectively, when R is varied from 50 Ω to 100 Ω by keeping the other parameter values the same as in Table 3. It can be seen that the NGD center frequency is insensitive to R. However, the GD optimal absolute value and transmission coefficient optimal value at f_0 = 3.6 GHz are decreasing when R increases. The results of the other parametric analysis versus TL characteristic impedance, Z, are shown in Figure 7. Figures 7(a), (b) and (c) display the cartographies of GD, S_{11} and S_{21} when Z is varied from 0.5 kΩ to 1.5 kΩ by keeping the other parameters same as in Table 3. Once again, the NGD center frequency is insensitive to Z. The GD optimal absolute value and transmission coefficient optimal value at f_0 = 3.6 GHz behave inversely to the case of resistor variation.

After calculations and slight optimization of TL width and length, the NGD POC operating at 3.6 GHz was designed with the parameters indicated in Table 4.

Figure 8 display the compared results from calculations ("Calc.") and ADS® simulations ("Simu."). As expected theoretically, the BP NGD function is observed as depicted in Figure 8(a): the NGD centre frequency is of about f_0 = 3.6 GHz. Table 5 summarizes the differences between the Matlab calculated and ADS® simulated results. Figure 8(b) presents a comparison between the transmission coefficients. It can be seen that the loss is higher around the NGD centre frequency. Nevertheless, as depicted in Figure 8(c), the circuit is well-matched, i.e. S11 better than −10 dB over the frequency band. The slight deviation between the calculation and simulation
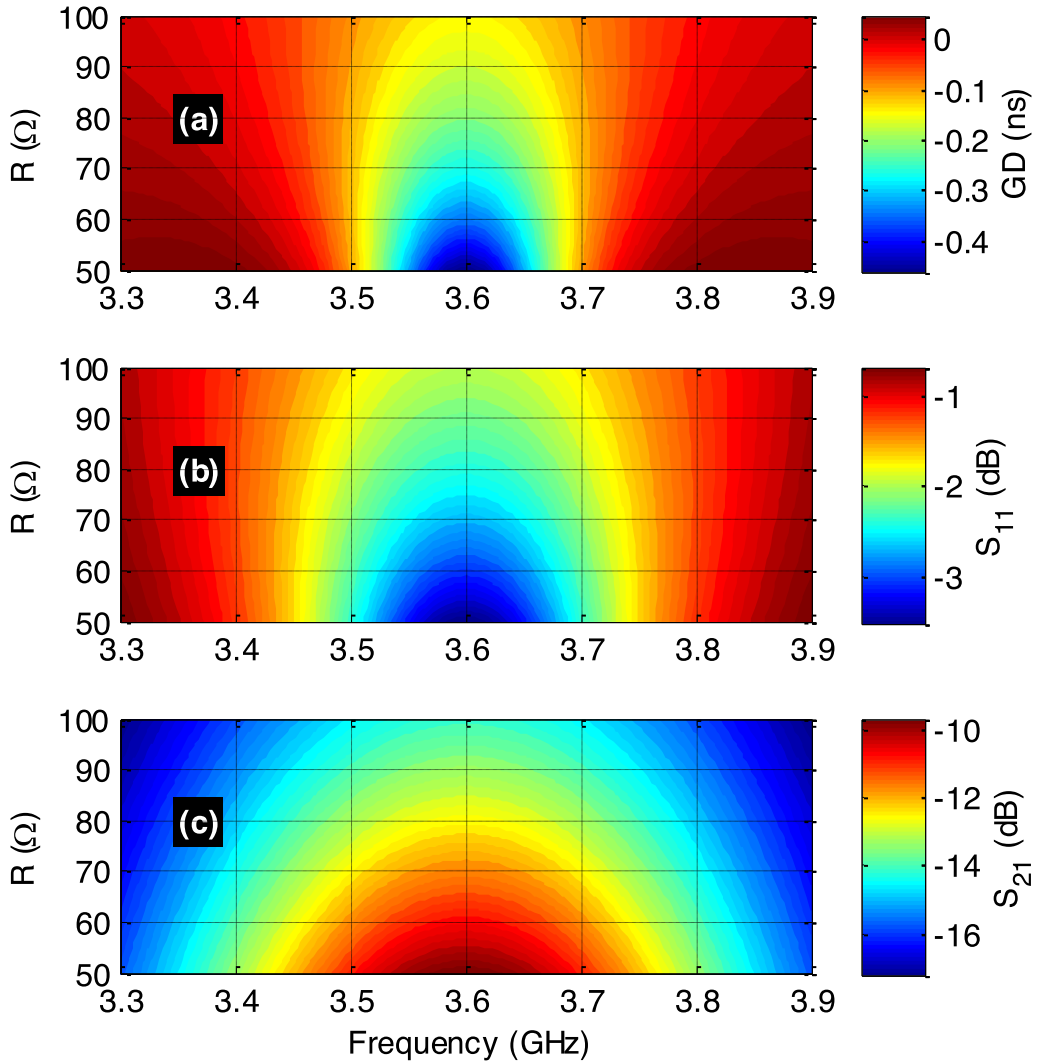
Figure 6. Parametric analyses of (a) GD, (b) S_{21} and (c) S_{11} versus (f, R).

Table 5. Characteristic of ideal and simulated NGD POCs

Characteristics	f_0 (GHz)	GD(f_0) (ns)	Δf (MHz)	S_{21} (f_0) (dB)	S_{11} (f_0) (dB)
Ideal	3.6	−0.34	327	−3.025	−10.63
Simu.	3.599	−0.298	172	−2.35	−12.67

herein is due to the skin effect and the substrate diffraction induced in the numerical simulation. Those effects are not included in the ideal model of our circuit in the S-matrix of (16).

4.2.2. *5.25-GHz BP NGD POC*

Table 6 summarizes the desired NGD specifications to design the 5G NGD POC to operate with 5.25 GHz centre frequency with respect to the US UNII standard [34]. The calculated NGD parameters by using design (37), (40) and (42) are given in Table 6.
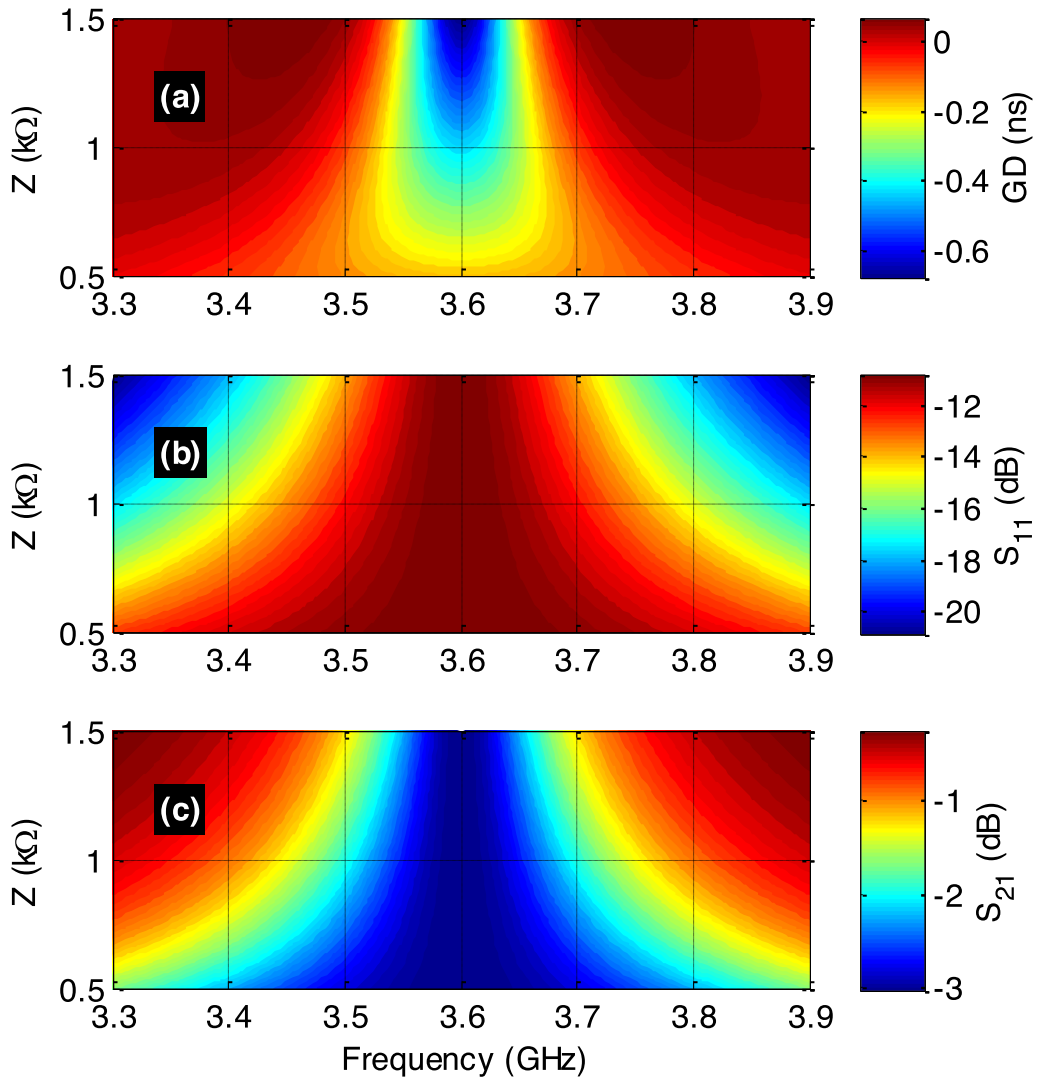
Figure 7. Parametric analyses of (a) GD, (b) S_{21} and (c) S_{11} versus (f, Z).

Table 6. NGD specifications and calculated parameters of the considered POC

Specifications	Designation	f_0	t	$-a_{\mathrm{dB}}$
	Value	5.25 GHz	0.23 ns	10 dB
NGD ideal parameters	Designation	τ_0	R	Z
	Value	47.6 ps	60 Ω	1 kΩ

In this case, the *S*-parameter analyses were computed in the bandwidth with $f_{\min} = 4.9$ GHz and $f_{\max} = 5.6$ GHz under more than 200 sampling.

Similar to the previous case of $f_0 = 3.6$ GHz, Figures 9 present the parametric analysis results with respect to resistor, *R*, and Figures 10 present that of parameter, *Z*. The same BP NGD behaviors are found even the center frequency is increased up to 5.25 GHz.
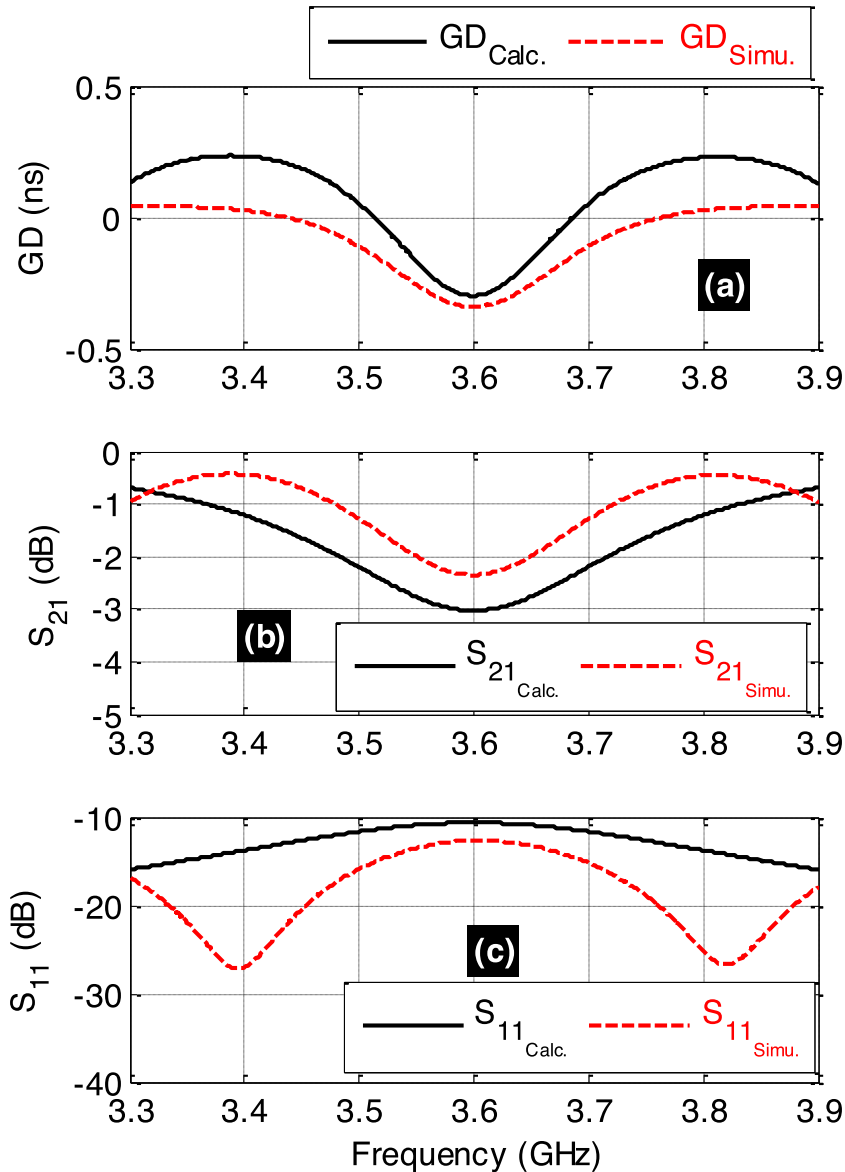
Figure 8. Calculated and simulated (a) GD, (b) S_{21} and (c) S_{11} of BP NGD circuit shown in Figure 5.

In an analogue way as in the previous case, the 5.25 GHz BP NGD POC was designed after calculations and slight optimization of TL width and length. The circuit was designed with the same parameters as indicated in Table 4 except the TL physical length, $d = 16$ cm.

Figure 11 illustrate the BP NGD behavior validation through theoretical and simulation results. Figure 11(a) presents a comparison between the calculated and simulated GDs. As expected, the NGD centre frequency is equal to $f_0 = 5.25$ GHz. Table 7 depicts the differences between the Matlab calculated and ADS® simulated results. Moreover, a good correlation between the calculated and simulated transmission and reflection coefficients are observed in Figures 11(b) and 11(c), respectively.
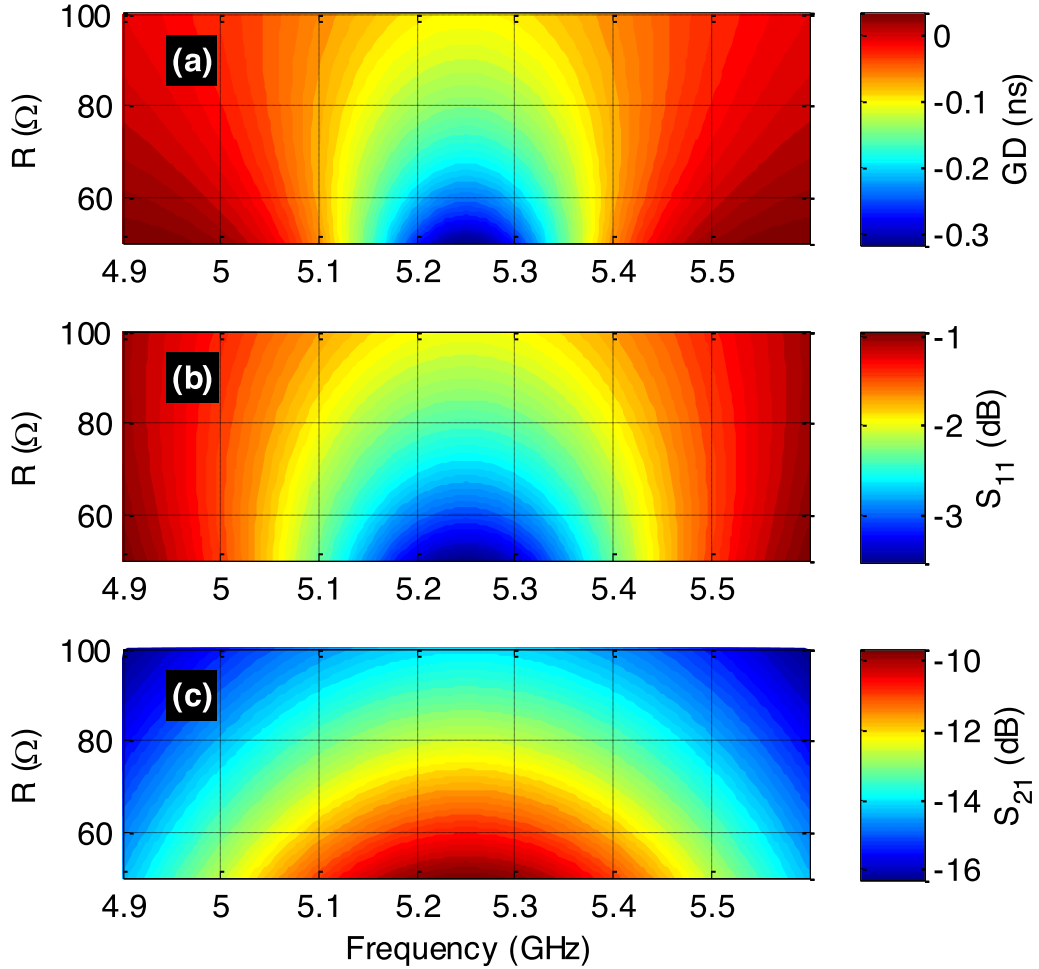
Figure 9. Parametric analyses of (a) GD, (b) S_{21} and (c) S_{11} versus (f, R).

Table 7. Characteristic of ideal and simulated NGD POCs

Characteristics	f_0 (GHz)	GD (f_0) (ns)	Δf (MHz)	S_{21} (f_0) (dB)	S_{11} (f_0) (dB)
Ideal	5.25	−0.334	470	−3.02	−10.6
Simu.	5.255	−0.2185	245	−2.447	−12.37

4.3. *Discussion on 5G applications*

The feasibility of the unfamiliar BP NGD function previously confirmed by the POC example raises questions on the ongoing research. The developed BP NGD concept led to think on a potential application for future design of RF and microwave devices.

4.3.1. *Tx–Rx architecture*

Among the different possibilities of application, we expect that the BP NGD responses can be used for the delay correction of multi-channel systems as the case of 802.11 a/b standards. One concrete scenario of application is illustrated by the network architecture of 5G displayed
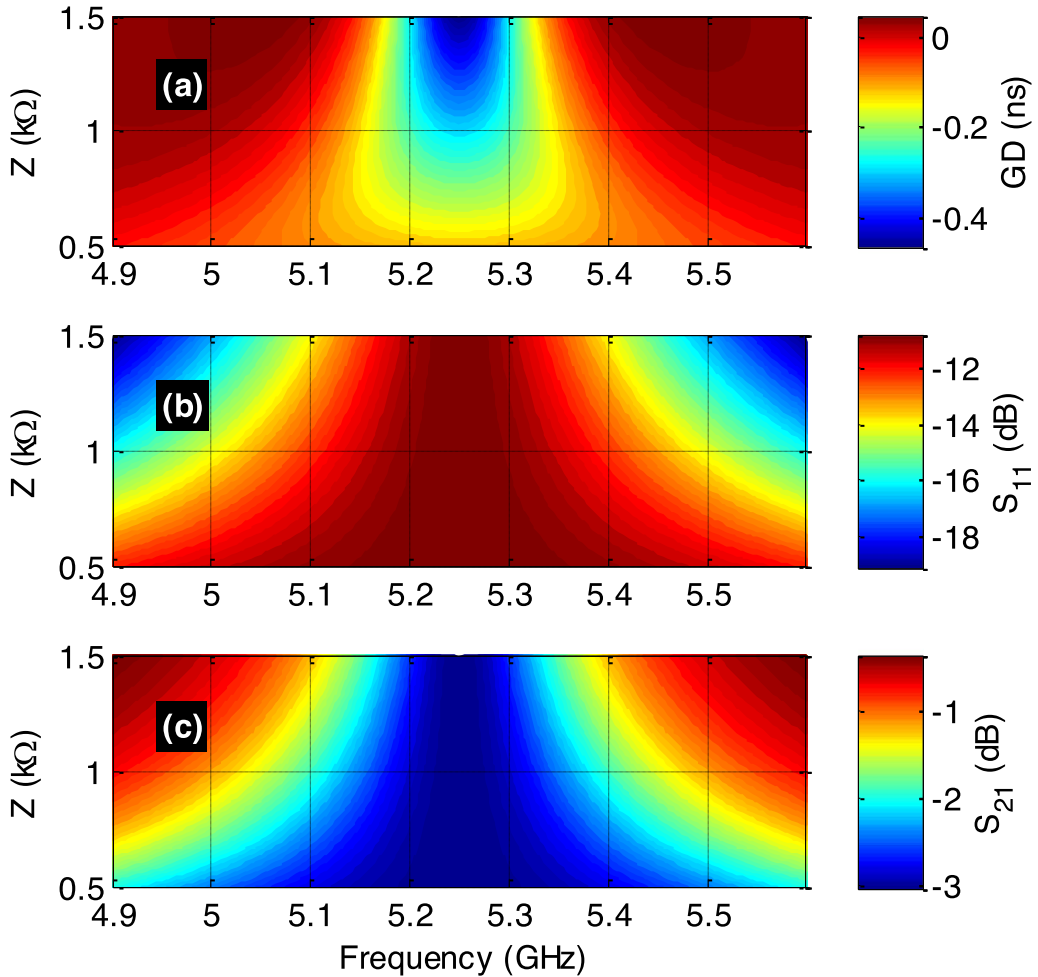
Figure 10. Parametric analyses of (a) GD, (b) S_{21} and (c) S_{11} versus (f, Z).

in Figure 12. Based on this scenario, we can imagine that multiple data can be transmitted from wireless communication standards as WiFi, GSM, LTE or 5G.

4.3.2. *Principle of differential delay correction with BP NGD function [21]*

In the more current cases of multiple connected objects, information can be transmitted from WSNs included in a Tx–Rx system. An example of WSN scenario and NGD delay effect reduction [20] between different channels, with centre frequencies-bandwidths, $(f_{m=1,2,3}, \Delta f_m)$, is illustrated in Figure 13(a). In the propagation environment with wave signal propagating at speed of light, $c = 300{,}000$ km/s, we can estimate the delay of the signal propagating from Tx(WS$_{m=1,2,3}$) point, M_m, to Rx point, M, by:
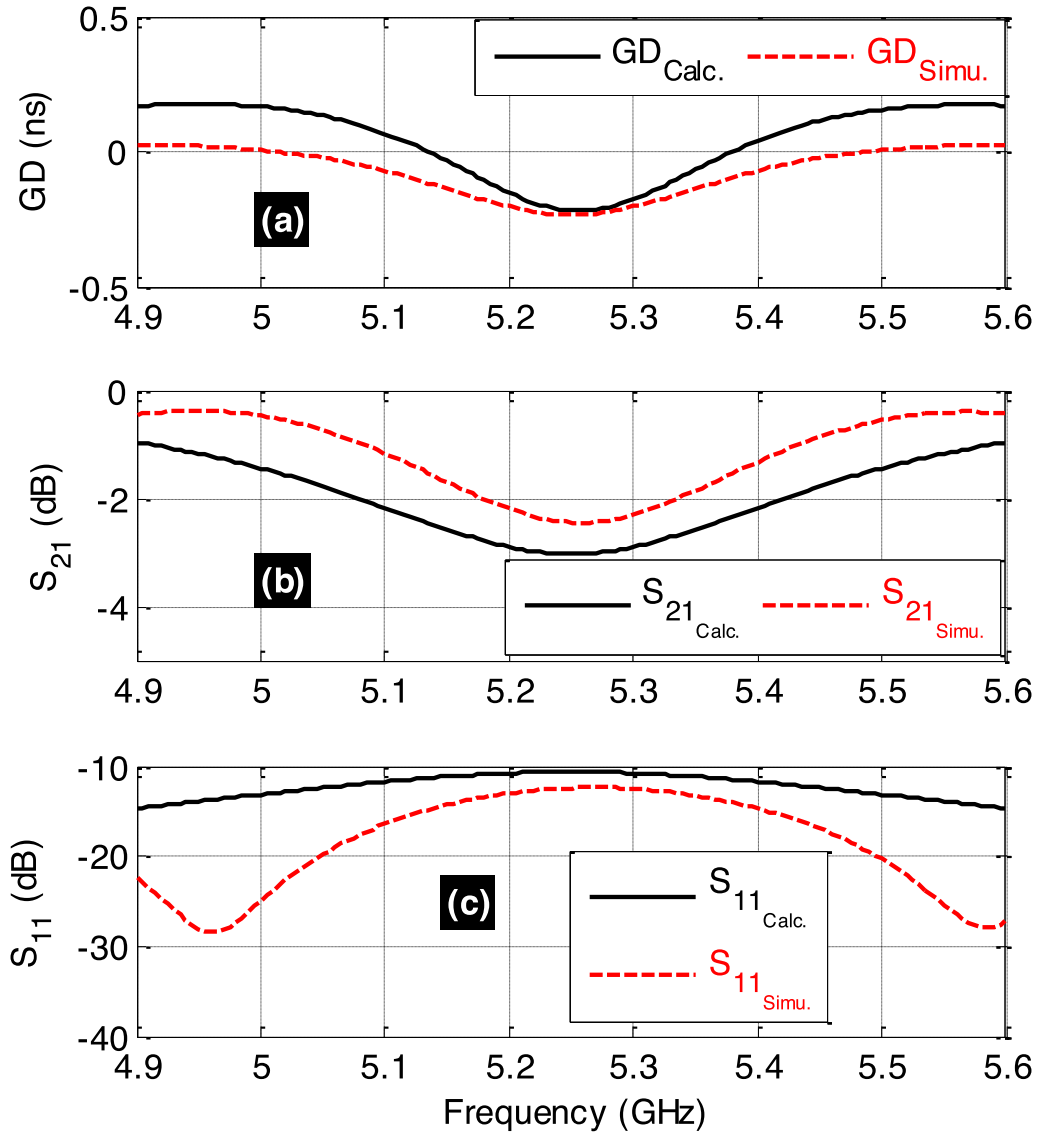
$$t_m(f_m) = \frac{d_m}{c}.$$

(43)

Figure 11. Calculated and simulated (a) GD, (b) S_{21} and (c) S_{11} of BP NGD POC operating with 5.25 GHz centre frequency.

In certain case of configuration as illustrated by Figure 9(a), we may consider delay differences:

$$\begin{cases} \Delta t_2 = t_2(f_2) - t_1(f_1) = \dfrac{d_2 - d_1}{c} \\ \Delta t_3 = t_3(f_3) - t_1(f_1) = \dfrac{d_3 - d_1}{c}. \end{cases} \tag{44}$$

Based on the innovative BP NGD function, a potential solution of delay difference inducing desynchronization between future 5G networks can be implemented with the configuration of Figure 13(b) [21]. It consists inserting a BP NGD function in the Rx system with, for example, dual
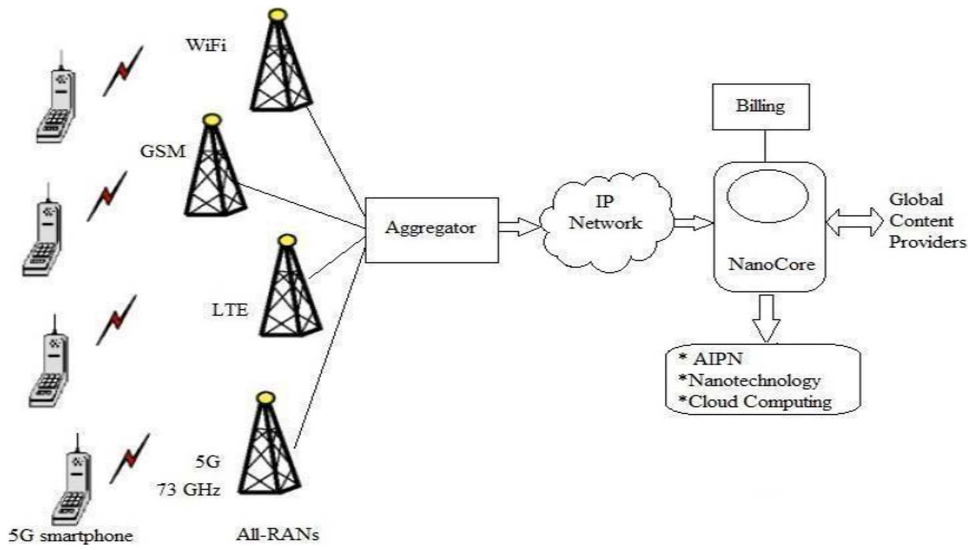
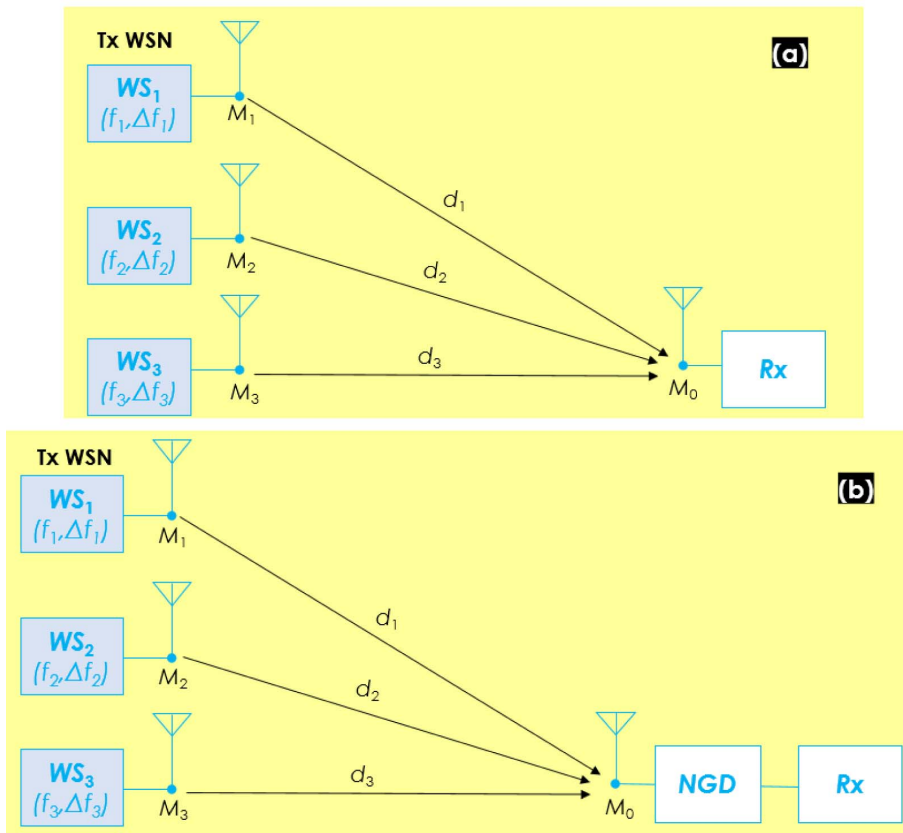**Figure 12.** Network Architecture for 5G [3].

Figure 13. Configuration NGD delay reduction [21].

band NGD aspect defined by:

$$\begin{cases} \mathrm{GD}(f_2) = \dfrac{d_1 - d_2}{c} \\ \mathrm{GD}(f_3) = \dfrac{d_1 - d_3}{c}. \end{cases} \tag{45}$$

In this case, assuming ideal matching between the Rx antenna, NGD circuit and input of the Rx system, the total delay for each channel can be expected as:

$$\begin{cases} \mathrm{delay}_{\mathrm{total}}(f_1) = \dfrac{d_1}{c} \\ \mathrm{delay}_{\mathrm{total}}(f_2) = t_2 + \mathrm{GD}(f_2) = \dfrac{d_1}{c} \\ \mathrm{delay}_{\mathrm{total}}(f_3) = t_3 + \mathrm{GD}(f_3) = \dfrac{d_1}{c}. \end{cases} \tag{46}$$

5. Conclusion

An investigation of BP NGD function generated with open-ended stub based passive topology is introduced. A pedagogical BP NGD theory is investigated. The basic specifications of the BP NGD function are introduced. The NGD circuit is constituted by a shunt parallel resistor ended by an open-ended stub. The NGD analysis and synthesis equations have been derived from the *S*-matrix equivalent model. The *S*-matrix model of the proposed topology is established based on the impedance matrix. The NGD analysis is realized from the expression of GD given by the assumed transmission coefficient. The synthesis formulas enabling to determine the considered topology parameters in function of the desired NGD specifications are proposed.

The validity of the BP NGD theory is verified with a POC of microstrip circuit operating around the 5G frequencies 3.6 GHz and 5.25 GHz. The promising *S*-parameters and GD results were obtained and discussed. As expected, results showing a BP NGD behaviour with a good correlation between calculation and commercial tool simulation is obtained. The obtained results are promising as an upcoming application of the BP NGD function for future developments related to 5G system delay correction.

References

[1] 5G Infrastructure Association, "5G PPP – The 5G infrastructure Public-Private Partnership", 2020, https://5g-ppp.eu/ (Permission granted to produce Figure 1), accessed dec. 2020.

[2] IEEE Spectrum, "The Race to 5G: The Latest 5G News and Analysis", 2019, https://spectrum.ieee.org/static/the-race-to-5g.

[3] S. Arunachalam, S. Kumar, H. Kshatriya, M. Patil, "Analyzing 5G: prospects of future technological advancements in mobile", *IOSR J. Eng.* **1** (2018), p. 6-11, International Conference on Innovative and Advanced Technologies in Engineering.

[4] Q. Yu, "The era of 5G and its impacts on EMC design and testing", in *Proceedings of IEEE International Symposium on EMC, SI/PI, Washington, DC, USA*, 2017, p. 7-11.

[5] V. Tikhvinskiy, A. Aitmagambetov, V. Koval, P. Korchagin, "Experimental test results of EMC between 5G and radio relay links in millimeter band", in *2019 International Symposium on Electromagnetic Compatibility - EMC EUROPE*, IEEE, 2019, p. 220-225.

[6] K. Wiklund, P. Stenumgaard, "EMC challenges for the era of massive internet of things", *IEEE Electromagn. Compat. Mag.* **8** (2019), no. 2, p. 65-74.

[7] J. Zhang, S. Zhang, Z. Ying, A. S. Morris, G. F. Pedersen, "Radiation-pattern reconfigurable phased array with p-i-n diodes controlled for 5G mobile terminals", *IEEE Trans. Microw. Theory Tech.* **68** (2020), no. 3, p. 1103-1117.

[8] V. Kallnichev, "Analysis of beam-steering and directive characteristics of adaptive antenna arrays for mobile communications", *IEEE Antennas Propag. Mag.* **43** (2001), no. 3, p. 145-152.

 [9] W. Alomar, A. Mortazawi, "Elimination of beam squint in uniformly excited serially fed antenna arrays using negative group delay circuits", in *Proceedings of IEEE International Symposium on Antennas and Propagation, Chicago, IL, USA, July 2012*, IEEE, 2012, p. 1-2.

[10] H. Mirzaei, G. V. Eleftheriades, "Arbitrary-angle squint-free beamforming in series-fed antenna arrays using non-foster elements synthesized by negative-group-delay networks", *IEEE Trans. Antennas Propag.* **63** (2015), no. 5, p. 1997-2010.

[11] A. Mortazawi, W. Alomar, "Negative group delay circuit", 2016, United States Patent Application US20160093958.

[12] M. Zhu, C.-T. M. Wu, "Reconfigurable series feed network for squint-free antenna beamforming using distributed amplifier-based negative group delay circuit", in *Proceedings of 2019 49th European Microwave Conference (EuMC), Paris, France, 1–3 October 2019*, IEEE, 2019, p. 256-259.

[13] W. Alomar, A. Mortazawi, "Method of generating negative group delay in phase arrays without using lossy circuits", in *Proceedings of IEEE Antennas and Propagation Wireless Symposium (IWS) 2013, Beijing, China, 14–18 April 2013*, IEEE, 2013, p. 1-4.

[14] H. Mirzaei, G. V. Eleftheriades, "Realizing non-Foster reactive elements using negative-group-delay networks", *IEEE Trans. Microw. Theory Tech.* **61** (2013), no. 12, p. 4322-4332.

[15] T. Zhang, R. Xu, C. M. Wu, "Unconditionally stable non-foster element using active transversal-filter-based negative group delay circuit", *IEEE Microw. Wirel. Compon. Lett.* **27** (2017), no. 10, p. 921-923.

[16] C. D. Broomfield, J. K. A. Everard, "Broadband negative group delay networks for compensation of oscillators, filters and communication systems", *Electron. Lett.* **36** (2000), no. 23, p. 1931-1933.

[17] B. Ravelo, "Distributed NGD active circuit for RF-microwave communication", *Int. J. Electron. Commun.* **68** (2014), no. 4, p. 282-290.

[18] L.-F. Qiu, L.-S. Wu, W.-Y. Yin, J.-F. Mao, "Absorptive bandstop filter with prescribed negative group delay and bandwidth", *IEEE Microw. Wirel. Compon. Lett.* **27** (2017), no. 7, p. 639-641.

[19] T. Shao, Z. Wang, S. Fang, H. Liu, Z. Chen, "A full-passband linear-phase band-pass filter equalized with negative group delay circuits", *IEEE Access* **8** (2020), p. 43336-43343.

[20] B. Ravelo, S. Lalléchère, A. Thakur, A. Saini, P. Thakur, "Theory and circuit modelling of baseband and modulated signal delay compensations with low- and band-pass NGD effects", *Int. J. Electron. Commun.* **70** (2016), no. 9, p. 1122-1127.

[21] F. Wan, N. Li, W. Rahajandraibe, B. Ravelo, "Reduction technique of differential propagation delay with negative group delay function", in *Proceedings of IEEE EuCAP 2020, Copenhagen, Denmark, 15–20 March 2020*, IEEE, 2020, p. 1-5.

[22] Z. Wang, Y. Cao, T. Shao, S. Fang, Y. Liu, "A negative group delay microwave circuit based on signal interference techniques", *IEEE Microw. Wirel. Compon. Lett.* **28** (2018), no. 4, p. 290-292.

[23] C.-T.-M. Wu, T. Itoh, "Maximally flat negative group-delay circuit: a microwave transversal filter approach", *IEEE Trans. Microw. Theory Tech.* **62** (2014), no. 6, p. 1330-1342.

[24] H. Choi, Y. Jeong, J. Lim, S. Y. Eom, Y. B. Jung, "A novel design for a dual-band negative group delay circuit", *IEEE Microw. Wirel. Compon. Lett.* **21** (2011), no. 1, p. 19-21.

[25] G. Chaudhary, Y. Jeong, J. Lim, "Miniaturized dual-band negative group delay circuit using dual-plane defected structures", *IEEE Microw. Wirel. Compon. Lett.* **24** (2014), no. 8, p. 521-523.

[26] G. Chaudhary, J. Jeong, P. Kim, Y. Jeong, J. Lim, "Compact negative group delay circuit using defected ground structure", in *2013 Asia-Pacific Microwave Conference Proceedings (APMC), Seoul*, IEEE, 2013, p. 22-24.

[27] G. Liu, J. Xu, "Compact transmission-type negative group delay circuit with low attenuation", *Electron. Lett.* **53** (2017), no. 7, p. 476-478.

[28] T. Shao, Z. Wang, S. Fang, H. Liu, S. Fu, "A compact transmission line self-matched negative group delay microwave circuit", *IEEE Access* **5** (2017), p. 22836-22843.

[29] G. Chaudhary, Y. Jeong, J. Lim, "Miniaturized dual-band negative group delay circuit using dual-plane defected structures", *IEEE Microw. Wirel. Compon. Lett.* **21** (2011), no. 1, p. 19-21.

[30] T. Shao, S. Fang, Z. Wang, H. Liu, "A compact dual-band negative group delay microwave circuit", *Radio Eng.* **27** (2018), no. 4, p. 1070-1076.

[31] B. Ravelo, "Similitude between the NGD function and filter gain behaviours", *Int. J. Circ. Theor. Appl.* **42** (2014), no. 10, p. 1016-1032.

[32] B. Ravelo, "On the low-pass, high-pass, bandpass and stop-band NGD RF passive circuits", *URSI Radio Sci. Bull.* **2017** (2017), no. 363, p. 10-27.

[33] B. Ravelo, S. Lalléchère, "FUTURE NETWORKS: 5G AND BEYOND. Design of 3.6-GHz 5G NGD passive circuit", 2020, 20e Journées Scientifiques URSI-France (JS'20), Future Network: 5G and Beyond, march 2020, Paris, France. https://hal.archives-ouvertes.fr/hal-02814577.

[34] Aruba Network, "802.11ac In-Depth", 2014, 37 pages, https://www.arubanetworks.com/assets/wp/WP_80211acInDepth.pdf.